SCIENCE CHINA
Technological Sciences

Special Topic: Current Progress in Solid Mechanics and Physical Mechanics
•Article•

May 2019 Vol.62 No.5: 736–746
https://doi.org/10.1007/s11431-018-9393-4

Mean-field homogenization of elasto-viscoplastic composites based on a new mapping-tangent linearization approach

YU Chao[1], KANG GuoZheng[1*] & FANG DaiNing[2]

[1] *Applied Mechanics and Structure Safety Key Laboratory of Sichuan Province, School of Mechanics and Engineering, Southwest Jiaotong University, Chengdu 610031, China;*
[2] *Institute of Advanced Technology, Beijing Institute of Technology, Beijing 100081, China*

Received October 10, 2018; accepted November 15, 2018; published online April 3, 2019

In this work, a new homogenization method of elasto-viscoplastic composites is developed. Using the fully implicit backward Euler's integration algorithm, the nonlinear ordinary differential equations in the constitutive laws of the matrix and inclusion phases are discretized. Three classical incremental linearization approaches, i.e., direct, secant and tangent ones are adopted and an affine relationship between the stress and strain increments is deduced. In order to reduce the interaction between the inclusion and matrix phases, a second-ordered mapping tensor is introduced and a new mapping-tangent linearization approach is proposed. Different linearization approaches are implemented by the incremental self-consistent scheme to predict the overall stress-strain response of particle-reinforced composites. It is shown that the predicted stress-strain curves given by the proposed mapping-tangent linearization approach are softer than that by other three classical ones, and are much closer to that from a full-field finite element simulation. Moreover, the linearized elasto-viscoplastic constitutive equation based on the proposed mapping-tangent approach has the same mathematical structure as the rate-independent elasto-plastic constitutive law. In this sense, the homogenization problems faced in the elasto-plastic and elasto-viscoplastic heterogeneous materials can be unified.

micromechanics, composites, elastic-viscoplasticity, self-consistent method, mapping-tangent linearization approach

Citation: Yu C, Kang G Z, Fang D N. Mean-field homogenization of elasto-viscoplastic composites based on a new mapping-tangent linearization approach. Sci China Tech Sci, 2019, 62: 736–746, https://doi.org/10.1007/s11431-018-9393-4

1 Introduction

Owing to low computational cost, mean-field homogenization approaches based on the Eshelby's inclusion theory [1] have been widely used to obtain the effective behaviors of heterogeneous materials (including composites and polycrystalline aggregates) within the framework of micromechanics. Two well-known mean-field homogenization approaches are the self-consistent [2] and Mori-Tanaka's [3] ones, firstly constructed to obtain the overall elastic property and further extended to describe the elasto-plastic and viscoplastic deformations of heterogeneous materials [4–12]. It should be noted that elasto-plastic constitutive law can be linearized as a rate form, i.e., $\dot{\boldsymbol{\varepsilon}} = \mathbf{M}^{\tan} : \dot{\boldsymbol{\sigma}}$, where $\dot{\boldsymbol{\varepsilon}}$ and $\dot{\boldsymbol{\sigma}}$ are the strain and stress rate tensors, respectively, and $\mathbf{M}^{\tan}$ is the tangent compliance tensor. However, in the case of viscoelasticity or elasto-viscoplasticity, the problems faced in the process of homogenization become more complex, since the strain rate depends on the stress and stress rate, simultaneously.

In the last few decades, much effort had been done to develop efficient homogenization method for modelling the viscoelastic and elasto-viscoplastic deformations of heterogeneous materials. The existing works can be classified into three groups: (1) the approach based on Laplace transfor-

*Corresponding author (email: guozhengkang@home.swjtu.edu.cn; guozhengkang@126.com)

mation [13–15]. In this approach, the linearized elasto-viscoplastic constitutive laws were firstly transformed into the Laplace-Carson space and a fictitious linear thermo-elastic relationship between stress and strain could be obtained. Then, the classical homogenization schemes (e.g., the self-consistent or Mori-Tanaka's ones) were adopted to estimate the interactions among different phases in the Laplace-Carson space. Finally, an inverse Laplace transformation was performed to obtain the macroscopic overall responses in the real time space. Although this approach reasonably considered the interactions among different phases in the heterogeneous materials, high computational time cost during the reverse Laplace transformation limits its further applications, especially for the long-time creep or cyclic deformation. (2) The approach based on the additive interaction law [16–22]. In this approach, the elasto-viscoplastic Eshelby's problem was viewed as an additive combination of two sub-problems, i.e., an elastic inclusion embedded in an elastic equivalent medium and a viscoplastic inclusion embedded in a viscoplastic equivalent medium. The Eshelby's tensors in the elastic and viscoplastic parts were determined by the elastic modulus and viscoplastic secant or tangent modulus, respectively. The interaction law could be regarded as a simple sum of interaction laws for elasticity [4] and viscoplasticity [8]. Thus, such an interaction law is an approximate method. Although the interactions among the different phases caused by elasticity and viscoplasticity were separately considered, such an approach overcome the shortcoming of high computational time cost faced during the reverse Laplace transformation, and has been widely used to describe the time-dependent deformation of heterogeneous materials. (3) The approach proposed by Doghri et al. [23–25] which coupled with numerical algorithms. Here, the elasto-viscoplastic constitutive laws were discretized by adopting the fully implicit backward Euler's integration algorithm. Then, the evolution equations of inelastic strain and internal variables at the beginning of each time interval were linearized around the ending time of the same interval [23]. After linearization, a tangent operator and an affine relationship between the stress and strain increments could be obtained. This affine relationship has the same mathematical structure with the linear thermo-elastic problem and can be easily implemented by the classical incremental homogenization schemes (e.g., self-consistent or Mori-Tanka's ones) without introducing new interaction law. Besides the low computational cost, such an approach has a solid physical background since the interactions among different phases caused by elastic and viscoplastic deformations are considered, simultaneously. It should be noted that although a new proposed tangent operator is adopted to derive the interaction law, the predicted stress-strain responses are still stiffer than that given by the mean-field homogenization approach based on the Laplace transformation and full-field finite element simulation, especially in the case at high strain rate [23].

The aim of this work is to develop a new mean-field homogenization approach coupled with numerical algorithms, which can reasonably reduce the interaction between inclusion and matrix phases and describe the nonlinear elasto-viscoplastic deformation of composites more reasonably. Following the idea of Doghri et al. [23], the nonlinear ordinary differential equations in the constitutive laws of matrix and inclusion phases are discretized by adopting the fully implicit backward Euler's integration algorithm. Then, three classical linearization approaches, i.e., direct, secant and tangent ones are adopted and affine relationships between the stress and strain increments are deduced. Incremental self-consistent scheme is used to estimate the interaction between the inclusion and matrix phases. It is shown that the predicted macroscopic stress-strain curves given by different linearization approaches almost coincide with each other but stiffer than that by the full-field finite element simulations. In order to obtain a softer response, a second-ordered mapping tensor is introduced and a new mapping-tangent linearization approach is proposed. The macroscopic stress-strain responses predicted by the new proposed linearization approach is much closer to that from the full-field finite element simulations.

2 Linearization of nonlinear constitutive equations

As discussed by Hill [4], the nonlinear ordinary differential equations in the elasto-plastic constitutive law can be linearized as a unified form, i.e., $\dot{\boldsymbol{\varepsilon}} = \mathbf{M}^{\tan} : \dot{\boldsymbol{\sigma}}$. However, in the case of elasto-viscoplasticity, the linearization approaches are not unique, and strongly influence the predicted overall stress-strain responses of the composites. Thus, in this section, the elasto-viscoplastic constitutive equations are linearized based on three classical (i.e., direct, secant and tangent ones) and a new proposed mapping-tangent linearization approaches, respectively.

The elasto-viscoplastic constitutive equations can be written as the following general form:

$$\dot{\boldsymbol{\varepsilon}} = \dot{\boldsymbol{\varepsilon}}^{\mathrm{e}} + \dot{\boldsymbol{\varepsilon}}^{\mathrm{p}}, \tag{1a}$$

$$\dot{\boldsymbol{\varepsilon}}^{\mathrm{e}} = \mathbf{M}^{\mathrm{e}} : \dot{\boldsymbol{\sigma}}, \tag{1b}$$

$$\dot{\boldsymbol{\varepsilon}}^{\mathrm{p}} = \bar{\boldsymbol{\varepsilon}}(\boldsymbol{\sigma}, R), \tag{1c}$$

$$\dot{R} = \tilde{R}(\dot{\boldsymbol{\varepsilon}}^{\mathrm{p}}, R), \tag{1d}$$

where $\dot{\boldsymbol{\varepsilon}}^{\mathrm{e}}$ and $\dot{\boldsymbol{\varepsilon}}^{\mathrm{p}}$ are the elastic and plastic strain rate tensors, respectively. $\mathbf{M}^{\mathrm{e}}$ is the elastic compliance tensor, R is the resistance of plastic deformation and is used to describe the isotropic hardening, $\bar{\boldsymbol{\varepsilon}}$ and $\tilde{R}$ are given functions defining the evolutions of $\boldsymbol{\varepsilon}^{\mathrm{p}}$ and R with respect to time t. It should be

pointed out that in this work, the back stress which is used to describe the kinematic hardening of plastic deformation is not considered for simplicity.

Now, consider a time interval $[t_n, t_{n+1}]$. It is assumed that at time t_n, all the variables are known. In this work, the increments are denoted as the symbol Δ, e.g., $\Delta t=t_{n+1}-t_n$. Eqs. (1a) to (1d) can be discretized by using a fully implicit backward Euler integration algorithm, i.e.,

$$\Delta\boldsymbol{\varepsilon} = \Delta\boldsymbol{\varepsilon}^{\mathrm{e}} + \Delta\boldsymbol{\varepsilon}^{\mathrm{p}}, \tag{2a}$$

$$\Delta\boldsymbol{\varepsilon}^{\mathrm{e}} = \mathbf{M}^{\mathrm{e}} : \Delta\boldsymbol{\sigma}, \tag{2b}$$

$$\Delta\boldsymbol{\varepsilon}^{\mathrm{p}} = \tilde{\boldsymbol{\varepsilon}}(\boldsymbol{\sigma}_{n+1}, R_{n+1})\Delta t, \tag{2c}$$

$$\Delta R = \tilde{R}\left(\frac{\Delta\boldsymbol{\varepsilon}^{\mathrm{p}}}{\Delta t}, R_{n+1}\right)\Delta t. \tag{2d}$$

The following notations are introduced:

$$\tilde{\boldsymbol{\varepsilon}}_{n+1} = \tilde{\boldsymbol{\varepsilon}}(\boldsymbol{\sigma}_{n+1}, R_{n+1}), \tag{3a}$$

$$\tilde{R}_{n+1} = \tilde{R}\left(\frac{\Delta\boldsymbol{\varepsilon}^{\mathrm{p}}}{\Delta t}, R_{n+1}\right), \tag{3b}$$

$$\tilde{\boldsymbol{\varepsilon}}_{n} = \tilde{\boldsymbol{\varepsilon}}(\boldsymbol{\sigma}_{n}, R_{n}), \tag{3c}$$

$$\tilde{R}_{n} = \tilde{R}(\mathbf{0}, R_{n}), \tag{3d}$$

where three classical linearization approaches, i.e., direct, secant tangent ones are adopted.

Direct approach

$$\Delta\boldsymbol{\varepsilon} = \mathbf{M}^{\mathrm{e}} : \Delta\boldsymbol{\sigma} + \Delta\boldsymbol{\varepsilon}^{\mathrm{p}}. \tag{4}$$

Secant approach

$$\begin{aligned}\Delta\boldsymbol{\varepsilon} &= \mathbf{M}^{\mathrm{e}} : \Delta\boldsymbol{\sigma} + \tilde{\boldsymbol{\varepsilon}}_{n+1}\Delta t \\ &= \mathbf{M}^{\mathrm{e}} : \Delta\boldsymbol{\sigma} + \left(\tilde{\boldsymbol{\varepsilon}}_{n+1}\otimes\boldsymbol{\sigma}_{n+1}^{-1}\Delta t\right) : \boldsymbol{\sigma}_{n+1} \\ &= \left[\mathbf{M}^{\mathrm{e}} + \left(\tilde{\boldsymbol{\varepsilon}}_{n+1}\otimes\boldsymbol{\sigma}_{n+1}^{-1}\Delta t\right)\right] : \Delta\boldsymbol{\sigma} \\ &\quad + \left(\tilde{\boldsymbol{\varepsilon}}_{n+1}\otimes\boldsymbol{\sigma}_{n+1}^{-1}\Delta t\right) : \boldsymbol{\sigma}_{n}.\end{aligned} \tag{5}$$

Tangent approach: it is much more complex than the direct and secant ones. The evolution equations of $\boldsymbol{\varepsilon}^{\mathrm{p}}$ and R (eqs. (1c) and (1d)) can be linearized at time t_n around time t_{n+1} through the Taylor's series expansion. Neglecting the second-ordered small quantity, it yields

$$\tilde{\boldsymbol{\varepsilon}}_{n} = \tilde{\boldsymbol{\varepsilon}}_{n+1} - \frac{\partial\tilde{\boldsymbol{\varepsilon}}_{n+1}}{\partial\boldsymbol{\sigma}_{n+1}} : \Delta\boldsymbol{\sigma} - \frac{\partial\tilde{\boldsymbol{\varepsilon}}_{n+1}}{\partial R_{n+1}}\Delta R, \tag{6a}$$

$$\tilde{R}_{n} = \tilde{R}_{n+1} - \frac{\partial\tilde{R}_{n+1}}{\partial\Delta\boldsymbol{\varepsilon}^{\mathrm{p}}} : \Delta\boldsymbol{\varepsilon}^{\mathrm{p}} - \frac{\partial\tilde{R}_{n+1}}{\partial R_{n+1}}\Delta R. \tag{6b}$$

By eqs. (6a) and (6b), it yields

$$\Delta R = \left(\frac{1}{\Delta t} - \frac{\partial\tilde{R}_{n+1}}{\partial R_{n+1}}\right)^{-1}\left(\tilde{R}_{n} + \frac{\partial\tilde{R}_{n+1}}{\partial\Delta\boldsymbol{\varepsilon}^{\mathrm{p}}} : \Delta\boldsymbol{\varepsilon}^{\mathrm{p}}\right), \tag{7a}$$

$$\begin{aligned}\tilde{\boldsymbol{\varepsilon}}_{n+1} &= \tilde{\boldsymbol{\varepsilon}}_{n} + \frac{\partial\tilde{\boldsymbol{\varepsilon}}_{n+1}}{\partial\boldsymbol{\sigma}_{n+1}} : \Delta\boldsymbol{\sigma} \\ &\quad + \frac{\partial\tilde{\boldsymbol{\varepsilon}}_{n+1}}{\partial R_{n+1}}\left(\frac{1}{\Delta t} - \frac{\partial\tilde{R}_{n+1}}{\partial R_{n+1}}\right)^{-1}\left(\tilde{R}_{n} + \frac{\partial\tilde{R}_{n+1}}{\partial\Delta\boldsymbol{\varepsilon}^{\mathrm{p}}} : \Delta\boldsymbol{\varepsilon}^{\mathrm{p}}\right).\end{aligned} \tag{7b}$$

Combining eqs. (7b) with (2a), the linearized constitutive equation can be obtained:

$$\begin{aligned}\Delta\boldsymbol{\varepsilon} &= \left(\mathbf{M}^{\mathrm{e}} + \mathbf{A}^{-1} : \frac{\partial\tilde{\boldsymbol{\varepsilon}}_{n+1}}{\partial\boldsymbol{\sigma}_{n+1}}\right) : \Delta\boldsymbol{\sigma} \\ &\quad + \mathbf{A}^{-1} : \left[\tilde{\boldsymbol{\varepsilon}}_{n} + \frac{\partial\tilde{\boldsymbol{\varepsilon}}_{n+1}}{\partial R_{n+1}}\left(\frac{1}{\Delta t} - \frac{\partial\tilde{R}_{n+1}}{\partial R_{n+1}}\right)^{-1}\tilde{R}_{n}\right],\end{aligned} \tag{8}$$

where

$$\mathbf{A} = \frac{\mathbf{I}}{\Delta t} - \frac{\partial\tilde{\boldsymbol{\varepsilon}}_{n+1}}{\partial R_{n+1}}\left(\frac{1}{\Delta t} - \frac{\partial\tilde{R}_{n+1}}{\partial R_{n+1}}\right)^{-1} \otimes \frac{\partial\tilde{R}_{n+1}}{\partial\Delta\boldsymbol{\varepsilon}^{\mathrm{p}}}, \tag{9}$$

where $\mathbf{I}$ is the fourth-ordered unit tensor.

By eqs. (4), (5) and (9), it is seen that the relationships between the stress and strain increments given by different linearization approaches can be written as a uniform affine form:

$$\Delta\boldsymbol{\varepsilon} = \mathbf{M} : \Delta\boldsymbol{\sigma} + \Delta\boldsymbol{\varepsilon}^{\mathrm{b}}. \tag{10a}$$

For direct approach

$$\begin{aligned}\mathbf{M}^{\mathrm{dir}} &= \mathbf{M}^{\mathrm{e}}, \\ \Delta\boldsymbol{\varepsilon}^{\mathrm{b}}_{\mathrm{dir}} &= \Delta\boldsymbol{\varepsilon}^{\mathrm{p}}.\end{aligned} \tag{10b}$$

For secant approach

$$\begin{aligned}\mathbf{M}^{\mathrm{sec}} &= \mathbf{M}^{\mathrm{e}} + \left(\tilde{\boldsymbol{\varepsilon}}_{n+1}\otimes\boldsymbol{\sigma}_{n+1}^{-1}\Delta t\right), \\ \Delta\boldsymbol{\varepsilon}^{\mathrm{b}}_{\mathrm{sec}} &= \left(\tilde{\boldsymbol{\varepsilon}}_{n+1}\otimes\boldsymbol{\sigma}_{n+1}^{-1}\Delta t\right) : \boldsymbol{\sigma}_{n}.\end{aligned} \tag{10c}$$

For tangent approach

$$\begin{aligned}\mathbf{M}^{\mathrm{tan}} &= \mathbf{M}^{\mathrm{e}} + \mathbf{A}^{-1} : \frac{\partial\tilde{\boldsymbol{\varepsilon}}_{n+1}}{\partial\boldsymbol{\sigma}_{n+1}}, \\ \Delta\boldsymbol{\varepsilon}^{\mathrm{b}}_{\mathrm{tan}} &= \mathbf{A}^{-1} : \left[\tilde{\boldsymbol{\varepsilon}}_{n} + \frac{\partial\tilde{\boldsymbol{\varepsilon}}_{n+1}}{\partial R_{n+1}}\left(\frac{1}{\Delta t} - \frac{\partial\tilde{R}_{n+1}}{\partial R_{n+1}}\right)^{-1}\tilde{R}_{n}\right],\end{aligned} \tag{10d}$$

where $\mathbf{M}$ is the effective compliance tensor (e.g., elastic $\mathbf{M}^{\mathrm{dir}}$, secant $\mathbf{M}^{\mathrm{sec}}$ and tangent $\mathbf{M}^{\mathrm{tan}}$), $\Delta\boldsymbol{\varepsilon}^{\mathrm{b}}$ is a back-extrapolated term, named as affine strain increment.

In Sect. 4, the predictive capabilities of different linearization approaches will be discussed. However, it is shown that the predicted macroscopic stress-strain responses given by three classical linearization approaches almost coincide with each other but stiffer than that obtained from the full-field finite element simulation. In fact, the calculations performed in Sect. 4 show that in each loading step, the term $\Delta\mathbf{E}^{\mathrm{b}}$ is much larger than the term $\overline{\mathbf{M}} : \Delta\boldsymbol{\Sigma}$ when the plastic deformation is large. In other words, the classical linearization approaches result in that the strain increment $\Delta\mathbf{E}$ is dominated by $\Delta\mathbf{E}^{\mathrm{b}}$, rather than $\overline{\mathbf{M}} : \Delta\boldsymbol{\Sigma}$. Thus, the interaction between the matrix and inclusion phases is overestimated. This will be explained in details at the end of Sect. 3.

In order to overcome the aforementioned problems, a new mapping-tangent linearization approach is proposed in this work. The basic idea of such an approach is to eliminate the

back-extrapolated term through the introduction of a second-ordered mapping tensor.

The strain increment tensor can be written as

$$\begin{aligned}\Delta\boldsymbol{\varepsilon} &= \Delta\boldsymbol{\varepsilon}^{\mathrm{e}} + \Delta\boldsymbol{\varepsilon}^{\mathrm{p}} = \mathbf{M}^{\mathrm{e}} : \Delta\boldsymbol{\sigma} + \tilde{\boldsymbol{\varepsilon}}_{n+1}\Delta t \\ &= \left(\mathbf{M}^{\mathrm{e}} + \boldsymbol{\Gamma}\cdot\frac{\partial\tilde{\boldsymbol{\varepsilon}}_{n+1}}{\partial\boldsymbol{\sigma}_{n+1}}\Delta t\right) : \Delta\boldsymbol{\sigma} \\ &\quad + \left(\tilde{\boldsymbol{\varepsilon}}_{n+1} - \boldsymbol{\Gamma}\cdot\frac{\partial\tilde{\boldsymbol{\varepsilon}}_{n+1}}{\partial\boldsymbol{\sigma}_{n+1}} : \Delta\boldsymbol{\sigma}\right)\Delta t, \end{aligned} \tag{11}$$

where a new second-ordered mapping tensor $\boldsymbol{\Gamma}$ is introduced. From eq. (11), it is seen that the relationship between the stress and strain increments given by the new proposed linearization approach can also be written as a uniform affine form, like eq. (10a), i.e., mapping-tangent approach:

$$\begin{aligned}\mathbf{M}^{\mathrm{mtan}} &= \mathbf{M}^{\mathrm{e}} + \boldsymbol{\Gamma}\cdot\frac{\partial\tilde{\boldsymbol{\varepsilon}}_{n+1}}{\partial\boldsymbol{\sigma}_{n+1}}\Delta t, \\ \Delta\boldsymbol{\varepsilon}^{\mathrm{b}}_{\mathrm{mtan}} &= \left(\tilde{\boldsymbol{\varepsilon}}_{n+1} - \boldsymbol{\Gamma}\cdot\frac{\partial\tilde{\boldsymbol{\varepsilon}}_{n+1}}{\partial\boldsymbol{\sigma}_{n+1}} : \Delta\boldsymbol{\sigma}\right)\Delta t. \end{aligned} \tag{12}$$

To ensure $\Delta\boldsymbol{\varepsilon}^{\mathrm{b}} = \mathbf{0}$ (eliminate the back-extrapolated term), it requires

$$\tilde{\boldsymbol{\varepsilon}}_{n+1} - \boldsymbol{\Gamma}\cdot\frac{\partial\tilde{\boldsymbol{\varepsilon}}_{n+1}}{\partial\boldsymbol{\sigma}_{n+1}} : \Delta\boldsymbol{\sigma} = \mathbf{0}. \tag{13}$$

Then, the mapping tensor $\boldsymbol{\Gamma}$ can be determined by eq. (13)

$$\boldsymbol{\Gamma} = \tilde{\boldsymbol{\varepsilon}}_{n+1}\cdot\left(\frac{\partial\tilde{\boldsymbol{\varepsilon}}_{n+1}}{\partial\boldsymbol{\sigma}_{n+1}} : \Delta\boldsymbol{\sigma}_{n+1}\right)^{-1}. \tag{14}$$

It should be noted that a second-ordered tensor $\boldsymbol{\Gamma}$ is introduced in this work. In fact, the directions of $\frac{\partial\tilde{\boldsymbol{\varepsilon}}_{n+1}}{\partial\boldsymbol{\sigma}_{n+1}} : \Delta\boldsymbol{\sigma}$ and $\tilde{\boldsymbol{\varepsilon}}_{n+1}$ are not identical. Thus, $\boldsymbol{\Gamma}$ cannot be replaced by a scalar. Surely, higher ordered tensors (third or fourth) can also be adopted as the mapping tensor. However, eq. (13) only contains six independent algebraic equations. Once the higher ordered tensor is introduced, the number of unknowns is larger than that of the equations. In this case, additional assumptions for the direction of $\boldsymbol{\Gamma}$ are needed.

Once the back-extrapolated term is eliminated, the linearized stress-strain relationship can be written as $\Delta\boldsymbol{\varepsilon} = \mathbf{M}^{\mathrm{mtan}} : \Delta\boldsymbol{\sigma}$ ($\mathbf{M}^{\mathrm{mtan}}$ represents the ratio of the strain increment to the stress increment in each loading step), which has a same mathematical structure as the rate-independent elasto-plastic constitutive law. In this sense, the homogenization problems faced in the elasto-plastic and elasto-viscoplastic heterogeneous materials can be unified.

Figure 1 shows the effective compliance tensors and the affine strain increments given by the four different linearization methods. The relationships among the four compliance tensors and affine strain increments are $\|\mathbf{M}^{\mathrm{mtan}}\| > \|\mathbf{M}^{\mathrm{tan}}\| > \|\mathbf{M}^{\mathrm{sec}}\| > \|\mathbf{M}^{\mathrm{dir}}\|$ and $\left\|\Delta\boldsymbol{\varepsilon}^{\mathrm{b}}_{\mathrm{mtan}}\right\| < \left\|\Delta\boldsymbol{\varepsilon}^{\mathrm{b}}_{\mathrm{tan}}\right\| < \left\|\Delta\boldsymbol{\varepsilon}^{\mathrm{b}}_{\mathrm{sec}}\right\| < \left\|\Delta\boldsymbol{\varepsilon}^{\mathrm{b}}_{\mathrm{dir}}\right\|$.

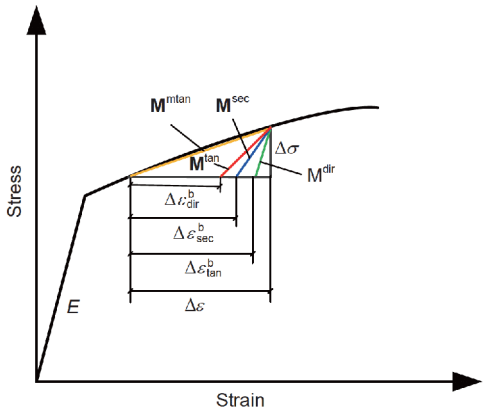

Figure 1 (Color online) Illustration of the four different linearization methods.

3 Self-consistent homogenization scheme

In this section, the incremental self-consistent homogenization scheme will be adopted to estimate the interaction between the inclusion and matrix phases. For simplicity, only the two-phase composites are considered in this work. It is assumed that each phase in the composites obeys an elasto-viscoplastic constitutive law. After linearization, their constitutive equations can be written as

$$\Delta\boldsymbol{\varepsilon}_{\mathrm{M}} = \mathbf{M}_{\mathrm{M}} : \Delta\boldsymbol{\sigma}_{\mathrm{M}} + \Delta\boldsymbol{\varepsilon}^{\mathrm{b}}_{\mathrm{M}}, \tag{15a}$$

$$\Delta\boldsymbol{\varepsilon}_{\mathrm{I}} = \mathbf{M}_{\mathrm{I}} : \Delta\boldsymbol{\sigma}_{\mathrm{I}} + \Delta\boldsymbol{\varepsilon}^{\mathrm{b}}_{\mathrm{I}}, \tag{15b}$$

where $\Delta\boldsymbol{\varepsilon}_{\mathrm{M}}$, $\Delta\boldsymbol{\sigma}_{\mathrm{M}}$, $\mathbf{M}_{\mathrm{M}}$ and $\Delta\boldsymbol{\varepsilon}^{\mathrm{b}}_{\mathrm{M}}$ are the average strain and stress increments, effective compliance tensor (including elastic, secant, tangent and mapping-tangent ones) and affine strain increment of matrix phase, respectively; while the terms $\Delta\boldsymbol{\varepsilon}_{\mathrm{I}}$, $\Delta\boldsymbol{\sigma}_{\mathrm{I}}$, $\mathbf{M}_{\mathrm{I}}$ and $\Delta\boldsymbol{\varepsilon}^{\mathrm{b}}_{\mathrm{I}}$ represent the corresponding variables of inclusion phase.

The macroscopic constitutive relationship of the composites can also be written as the following affine form:

$$\Delta\mathbf{E} = \overline{\mathbf{M}} : \Delta\boldsymbol{\Sigma} + \Delta\mathbf{E}^{\mathrm{b}}, \tag{16}$$

where $\Delta\mathbf{E}$, $\Delta\boldsymbol{\Sigma}$, $\overline{\mathbf{M}}$ and $\Delta\mathbf{E}^{\mathrm{b}}$ are the macroscopic overall strain and stress increments, effective compliance tensor and affine strain increment tensor of the composites, respectively.

Figure 2(a) shows a schematic view of a real composite made of inclusions embedded into the matrix phase. The composite is subjected to a macroscopic stress increment $\Delta\boldsymbol{\Sigma}$. In order to consider the interaction between the inclusion and matrix phases, the self-consistent homogenization scheme assumes that the real composite can be represented by an inclusion embedded in a homogeneous equivalent medium with an infinite volume. The homogeneous equivalent medium is subjected to the same stress increment $\Delta\boldsymbol{\Sigma}$ and its property is the same as the unknown macroscopic property of the composite, as shown in Figure 2(b).

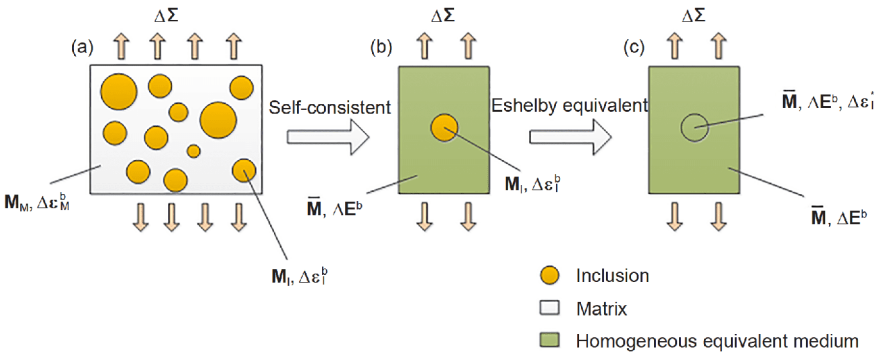

Figure 2 (Color online) Illustration of the incremental self-consistent homogenization approach. (a) The representative volume element (RVE) of the composite; (b) self-consistent homogenization; (c) the differences of the mechanical properties between the inclusion and matrix are simulated by the introduced eigenstrain.

According to the Eshelby's equivalent inclusion theory [1], the effective compliance tensor and the affine strain increment tensor of inclusion phase (i.e., $\mathbf{M}_I$ and $\Delta\boldsymbol{\varepsilon}_I^b$) can be replaced by those of homogeneous equivalent medium (i.e., $\overline{\mathbf{M}}$ and $\Delta\mathbf{E}^b$) once an artificially eigenstrain increment is introduced (as shown in Figure 2(c)). Then, the constitutive relationship of inclusion phase can be rewritten in the following equivalent form:

$$\Delta\boldsymbol{\varepsilon}_I = \overline{\mathbf{M}} : \Delta\boldsymbol{\sigma}_I + \Delta\mathbf{E}^b + \Delta\boldsymbol{\varepsilon}_I^*, \tag{17}$$

where $\Delta\boldsymbol{\varepsilon}_I^*$ is the introduced eigenstrain increment tensor.

By eqs. (16) and (17), it yields

$$\Delta\tilde{\boldsymbol{\varepsilon}}_I = \overline{\mathbf{M}} : \Delta\tilde{\boldsymbol{\sigma}}_I + \Delta\boldsymbol{\varepsilon}_I^*, \tag{18}$$

where $\Delta\tilde{\boldsymbol{\varepsilon}}_I$ and $\Delta\tilde{\boldsymbol{\sigma}}_I$ are the disturbance strain and stress increment tensors, respectively, i.e.,

$$\Delta\tilde{\boldsymbol{\varepsilon}}_I = \Delta\boldsymbol{\varepsilon}_I - \Delta\mathbf{E}, \tag{19a}$$

$$\Delta\tilde{\boldsymbol{\sigma}}_I = \Delta\boldsymbol{\sigma}_I - \Delta\boldsymbol{\Sigma}. \tag{19b}$$

The disturbance strain and eigenstrain increment tensors can be linked by the Eshelby's tensor $\boldsymbol{\Pi}$, i.e.,

$$\Delta\tilde{\boldsymbol{\varepsilon}}_I = \boldsymbol{\Pi} : \Delta\boldsymbol{\varepsilon}_I^*. \tag{20}$$

In general, the effective compliance tensor is not isotropic. In this case, the Eshelby's tensor can only be obtained by the numerical method which is very time consuming. As discussed by Doghri and Ouaar [9], Chaboche et al. [26] and Peng et al. [27], in the elastoplastic problem, a too stiff stress-strain response will be obtained once the anisotropic Eshelby's tensor is adopted. To soften the stress-strain response, Doghri and Ouaar [9] and Chaboche et al. [26] proposed some isotropization methods to obtain the isotropic Eshelby's tensor. Recently, Peng et al. [27] proposed a new and rational approach to determine the Eshelby's tensor of the elastoplastic medium, which has a solid physical background. The "too stiff" problem face in the elastoplastic composites have been solved by the works of Doghri and Ouaar [9], Chaboche et al. [26] and Peng et al. [27]. In this work, the isotropization method proposed by Doghri and Ouaar [9] is adopted, as

$$\bar{\nu} = \frac{3\bar{k} - 2\bar{\mu}}{2\left(3\bar{k} + \bar{\mu}\right)}, \tag{21a}$$

$$\bar{k} = \frac{1}{3}(\mathbf{I}^{\mathrm{vol}} :: \overline{\mathbf{M}}^{-1}), \tag{21b}$$

$$\bar{\mu} = \frac{1}{10}(\mathbf{I}^{\mathrm{dev}} :: \overline{\mathbf{M}}^{-1}), \tag{21c}$$

$$\mathbf{I}^{\mathrm{vol}} = \frac{1}{3}(\mathbf{1} \otimes \mathbf{1}), \tag{21d}$$

$$\mathbf{I}^{\mathrm{dev}} = \mathbf{I} - \mathbf{I}^{\mathrm{vol}}, \tag{21e}$$

where $\bar{\nu}$, $\bar{k}$ and $\bar{\mu}$ are the effective Poisson's ratio, bulk and shear moduli, respectively, and they are determined by the macroscopic effective compliance tensor $\overline{\mathbf{M}}$; $\mathbf{I}^{\mathrm{vol}}$ and $\mathbf{I}^{\mathrm{dev}}$ are the fourth-ordered unit spherical and deviatoric tensors, respectively, $\mathbf{1}$ is the second-ordered unit tensor, :: is an operator, i.e., $\mathbf{A} :: \mathbf{B} = A_{ijkl}B_{lkji}$ ($\mathbf{A}$ and $\mathbf{B}$ are two fourth-ordered tensors). Then, the Eshelby's tensor can be determined by the effective Poisson's ratio $\bar{\nu}$.

Substituting eq. (20) into eq. (18), the interaction law can be given as

$$\Delta\tilde{\boldsymbol{\varepsilon}}_I = -\widetilde{\mathbf{M}} : \Delta\tilde{\boldsymbol{\sigma}}_I, \tag{22}$$

where

$$\widetilde{\mathbf{M}} = (\mathbf{I} - \boldsymbol{\Pi})^{-1} : \boldsymbol{\Pi} : \overline{\mathbf{M}}, \tag{23}$$

is the interaction tensor.

Substituting eqs. (15b) and (16) into eq. (22), the following localization equation for the inclusion phase is obtained:

$$\Delta\boldsymbol{\sigma}_I = \mathbf{B}_I : \Delta\boldsymbol{\Sigma} + \mathbf{N}_I : \left(\Delta\mathbf{E}^b - \Delta\boldsymbol{\varepsilon}_I^b\right), \tag{24}$$

where the localization tensors $\mathbf{B}_I$ and $\mathbf{N}_I$ are defined as

$$\mathbf{B}_I = \left(\mathbf{M}_I + \widetilde{\mathbf{M}}\right)^{-1} : (\overline{\mathbf{M}} + \widetilde{\mathbf{M}}), \tag{25a}$$

$$\mathbf{N}_I = \left(\mathbf{M}_I + \widetilde{\mathbf{M}}\right)^{-1}. \tag{25b}$$

It is noted that the macroscopic strain and stress rates of two-phase composites can be written as the following rules of mixture:

$$f\Delta\boldsymbol{\sigma}_{\mathrm{I}}+(1-f)\Delta\boldsymbol{\sigma}_{\mathrm{M}}=\Delta\boldsymbol{\Sigma}, \tag{26a}$$

$$f\Delta\boldsymbol{\varepsilon}_{\mathrm{I}}+(1-f)\Delta\boldsymbol{\varepsilon}_{\mathrm{M}}=\Delta\mathbf{E}, \tag{26b}$$

or the equivalent form

$$f\Delta\tilde{\boldsymbol{\sigma}}_{\mathrm{I}}+(1-f)\Delta\tilde{\boldsymbol{\sigma}}_{\mathrm{M}}=\mathbf{0}, \tag{27a}$$

$$f\Delta\tilde{\boldsymbol{\varepsilon}}_{\mathrm{I}}+(1-f)\Delta\tilde{\boldsymbol{\varepsilon}}_{\mathrm{M}}=\mathbf{0}. \tag{27b}$$

Combining eq. (22) with eqs. (27a) and (27b) , it yields

$$\Delta\tilde{\boldsymbol{\varepsilon}}_{\mathrm{M}}=-\widetilde{\mathbf{M}}:\Delta\tilde{\boldsymbol{\sigma}}_{\mathrm{M}}. \tag{28}$$

Then, substituting eqs. (15a) and (16) into eq. (28), the following localization equation for the matrix phase is obtained:

$$\Delta\boldsymbol{\sigma}_{\mathrm{M}}=\mathbf{B}_{\mathrm{M}}:\Delta\boldsymbol{\Sigma}+\mathbf{N}_{\mathrm{M}}:\left(\Delta\mathbf{E}^{\mathrm{b}}-\Delta\boldsymbol{\varepsilon}_{\mathrm{M}}^{\mathrm{b}}\right), \tag{29}$$

where the localization tensors $\mathbf{B}_{\mathrm{M}}$ and $\mathbf{N}_{\mathrm{M}}$ are defined as

$$\mathbf{B}_{\mathrm{M}}=\left(\mathbf{M}_{\mathrm{M}}+\widetilde{\mathbf{M}}\right)^{-1}:(\overline{\mathbf{M}}+\widetilde{\mathbf{M}}), \tag{30a}$$

$$\mathbf{N}_{\mathrm{M}}=\left(\mathbf{M}_{\mathrm{M}}+\widetilde{\mathbf{M}}\right)^{-1}. \tag{30b}$$

Substituting eqs. (15a), (15b), (24) and (29) into eq. (26b), the macroscopic strain tensor can be written as

$$\begin{aligned}\Delta\mathbf{E}=&\left[f\mathbf{M}_{\mathrm{I}}:\mathbf{B}_{\mathrm{I}}+(1-f)\mathbf{M}_{\mathrm{M}}:\mathbf{B}_{\mathrm{M}}\right]:\Delta\boldsymbol{\Sigma}\\&+\left[f\mathbf{M}_{\mathrm{I}}:\mathbf{N}_{\mathrm{I}}+(1-f)\mathbf{M}_{\mathrm{M}}:\mathbf{N}_{\mathrm{M}}\right]:\Delta\mathbf{E}^{\mathrm{b}}\\&+\left[f(\mathbf{I}-\mathbf{M}_{\mathrm{I}}:\mathbf{N}_{\mathrm{I}}):\Delta\boldsymbol{\varepsilon}_{\mathrm{I}}^{\mathrm{b}}+(1-f)\right.\\&\left.\times(\mathbf{I}-\mathbf{M}_{\mathrm{M}}:\mathbf{N}_{\mathrm{M}}):\Delta\boldsymbol{\varepsilon}_{\mathrm{M}}^{\mathrm{b}}\right].\end{aligned} \tag{31}$$

Comparing eq. (31) with eq. (16), the macroscopic effective compliance tensor and affine strain increment tensor can be obtained as

$$\overline{\mathbf{M}}=f\mathbf{M}_{\mathrm{I}}:\mathbf{B}_{\mathrm{I}}+(1-f)\mathbf{M}_{\mathrm{M}}:\mathbf{B}_{\mathrm{M}}, \tag{32a}$$

$$\begin{aligned}\Delta\mathbf{E}^{\mathrm{b}}=&\left[\mathbf{I}-f\mathbf{M}_{\mathrm{I}}:\mathbf{N}_{\mathrm{I}}+(1-f)\mathbf{M}_{\mathrm{M}}:\mathbf{N}_{\mathrm{M}}\right]^{-1}\\&:\left[f(\mathbf{I}-\mathbf{M}_{\mathrm{I}}:\mathbf{N}_{\mathrm{I}}):\Delta\boldsymbol{\varepsilon}_{\mathrm{I}}^{\mathrm{b}}\right.\\&\left.+(1-f)(\mathbf{I}-\mathbf{M}_{\mathrm{M}}:\mathbf{N}_{\mathrm{M}}):\Delta\boldsymbol{\varepsilon}_{\mathrm{M}}^{\mathrm{b}}\right].\end{aligned} \tag{32b}$$

By eqs. (23) and (32a), it is seen that the interaction tensor $\widetilde{\mathbf{M}}$ is determined by the effective compliance tensors of the matrix and inclusion ($\mathbf{M}_{\mathrm{M}}$ and $\mathbf{M}_{\mathrm{I}}$). Let's consider two extreme situations, when $\mathbf{M}_{\mathrm{M}}\to\mathbf{0}$ and $\mathbf{M}_{\mathrm{I}}\to\mathbf{0}$, then $\widetilde{\mathbf{M}}\to\mathbf{0}$, by the interaction laws (eqs. (22) and (28)) it can be obtained that $\Delta\tilde{\boldsymbol{\varepsilon}}_{\mathrm{I}}\to\mathbf{0}$ and $\Delta\tilde{\boldsymbol{\varepsilon}}_{\mathrm{M}}\to\mathbf{0}$. That means the strain field in the composite tends to be uniform, i.e., the interaction between matrix and inclusion is overestimated and the predicted stress-strain response is much stiffer than the real one. When $\mathbf{M}_{\mathrm{M}}\to\infty$ and $\mathbf{M}_{\mathrm{I}}\to\infty$, then $\widetilde{\mathbf{M}}\to\infty$, it can be obtained that $\Delta\tilde{\boldsymbol{\sigma}}_{\mathrm{I}}\to\mathbf{0}$ and $\Delta\tilde{\boldsymbol{\sigma}}_{\mathrm{M}}\to\mathbf{0}$. That means the stress field in the composite tends to be uniform, i.e., the interaction between matrix and inclusion is underestimated and the predicted stress-strain response is much softer than the real one. Thus, an effective way to weaken the interaction between matrix and inclusion is to chosen a larger compliance tensor in a rational way.

As shown in Figure 1, since the mapping tangent compliance tensor $\mathbf{M}^{\mathrm{mtan}}$ is much larger than the other compliance tensors, i.e., $\mathbf{M}^{\mathrm{dir}}$, $\mathbf{M}^{\mathrm{sec}}$ and $\mathbf{M}^{\mathrm{tan}}$, the interaction between the matrix and inclusion can be weakened when $\mathbf{M}^{\mathrm{mtan}}$ is adopted.

4 Numerical simulations

In this section, the predicted stress-strain responses given by the self-consistent homogenization scheme based on different linearization approaches are compared with the full-field finite element simulations performed by Pierard et al. [15]. Thus, the constitutive equations used in this work are kept as the same as those in Pierard et al. [15]. The main equations are listed as follows:

$$\dot{\boldsymbol{\varepsilon}}=\dot{\boldsymbol{\varepsilon}}^{\mathrm{e}}+\dot{\boldsymbol{\varepsilon}}^{\mathrm{p}}, \tag{33a}$$

$$\dot{\boldsymbol{\varepsilon}}^{\mathrm{e}}=\mathbf{M}^{\mathrm{e}}:\dot{\boldsymbol{\sigma}}, \tag{33b}$$

$$f=\sqrt{3/2}\,\|\mathbf{s}\|-R, \tag{33c}$$

$$\dot{\boldsymbol{\varepsilon}}^{\mathrm{p}}=\begin{cases}\sqrt{\dfrac{3}{2}}\gamma_0\left(\dfrac{f}{R}\right)^m\dfrac{\mathbf{s}}{\|\mathbf{s}\|}, & f>0,\\ \mathbf{0}, & f\le 0,\end{cases} \tag{33d}$$

$$R=\sigma_Y+kp^d,$$

$$\dot{p}=\sqrt{\frac{2}{3}\dot{\boldsymbol{\varepsilon}}^{\mathrm{p}}:\dot{\boldsymbol{\varepsilon}}^{\mathrm{p}}},$$

where $\mathbf{s}$ is the deviatoric stress tensor, f is the yield surface, γ_0, k and d are three material parameters, m is the viscosity coefficient, when m is small/large, it represents for the strong/weak viscosity, p is the accumulated plastic strain.

Using the linearization approaches discussed above, the constitutive equations (eq. (33a)–(33d)) can be linearized as

$$\Delta\boldsymbol{\varepsilon}=\mathbf{M}:\Delta\boldsymbol{\sigma}+\Delta\boldsymbol{\varepsilon}^{\mathrm{b}}. \tag{34a}$$

Direct approach

$$\begin{aligned}&\mathbf{M}^{\mathrm{dir}}=\mathbf{M}^{\mathrm{e}},\\&\Delta\boldsymbol{\varepsilon}_{\mathrm{dir}}^{\mathrm{b}}=\Delta\boldsymbol{\varepsilon}^{\mathrm{p}}.\end{aligned} \tag{34b}$$

Secant approach

$$\begin{aligned}&\mathbf{M}^{\mathrm{sec}}=\mathbf{M}^{\mathrm{e}}+\sqrt{\frac{3}{2}}\gamma_0\left(\frac{f_{n+1}}{R_{n+1}}\right)^m\frac{\mathbf{I}^{\mathrm{dev}}\Delta t}{\|\mathbf{s}_{n+1}\|},\\&\Delta\boldsymbol{\varepsilon}_{\mathrm{sec}}^{\mathrm{b}}=\mathbf{M}^{\mathrm{p}}:\boldsymbol{\sigma}_n.\end{aligned} \tag{34c}$$

Tangent approach

$$
\begin{aligned}
&\mathbf{M}^{\tan}=\mathbf{M}^{\mathrm{e}}+\mathbf{A}^{-1}:\frac{\partial\tilde{\boldsymbol{\varepsilon}}_{n+1}}{\partial\boldsymbol{\sigma}_{n+1}},\\
&\mathbf{A}=\frac{\mathbf{I}}{\Delta t}-\frac{\partial\tilde{\boldsymbol{\varepsilon}}_{n+1}}{\partial R_{n+1}}\left(\frac{1}{\Delta t}-\frac{\partial\tilde{R}_{n+1}}{\partial R_{n+1}}\right)^{-1}\otimes\frac{\partial\tilde{R}_{n+1}}{\partial\Delta\boldsymbol{\varepsilon}^{\mathrm{p}}},\\
&\Delta\boldsymbol{\varepsilon}^{\mathrm{b}}_{\tan}=\mathbf{A}^{-1}:\left[\tilde{\boldsymbol{\varepsilon}}_{n}+\frac{\partial\tilde{\boldsymbol{\varepsilon}}_{n+1}}{\partial R_{n+1}}\left(\frac{1}{\Delta t}-\frac{\partial\tilde{R}_{n+1}}{\partial R_{n+1}}\right)^{-1}\tilde{R}_{n}\right],\\
&\frac{\partial\tilde{\boldsymbol{\varepsilon}}_{n+1}}{\partial R_{n+1}}=-\sqrt{\frac{3}{2}}\frac{m\gamma_0}{R_{n+1}}\left(\frac{f_{n+1}}{R_{n+1}}\right)^{m}\frac{\mathbf{s}_{n+1}}{\|\mathbf{s}_{n+1}\|},\\
&\frac{\partial\tilde{R}_{n+1}}{\partial R_{n+1}}=0,\\
&\frac{\partial\tilde{R}_{n+1}}{\partial\Delta\boldsymbol{\varepsilon}^{\mathrm{p}}}=\sqrt{\frac{2}{3}}\,dkp_{n}^{d-1}\frac{\Delta\boldsymbol{\varepsilon}^{\mathrm{p}}}{\|\Delta\boldsymbol{\varepsilon}^{\mathrm{p}}\|}.
\end{aligned}
\tag{34d}
$$

Mapping-tangent approach

$$
\begin{aligned}
\mathbf{M}^{\mathrm{mtan}}=&\mathbf{M}^{\mathrm{e}}+\frac{3}{2}\frac{m\gamma_0\Delta t}{R_{n+1}}\left(\frac{f_{n+1}}{R_{n+1}}\right)^{m-1}\boldsymbol{\Gamma}\cdot\mathbf{N}_{n+1}\otimes\mathbf{N}_{n+1}\\
&+\sqrt{\frac{3}{2}}\gamma_0\Delta t\left(\frac{f_{n+1}}{R_{n+1}}\right)^{m}\frac{\boldsymbol{\Gamma}\cdot\left(\mathbf{I}^{\mathrm{dev}}-\mathbf{N}_{n+1}\otimes\mathbf{N}_{n+1}\right)}{\|\mathbf{s}_{n+1}\|},\\
\mathbf{N}_{n+1}=&\frac{\mathbf{s}_{n+1}}{\|\mathbf{s}_{n+1}\|},\\
\Delta\boldsymbol{\varepsilon}^{\mathrm{b}}_{\mathrm{mtan}}=&\left(\tilde{\boldsymbol{\varepsilon}}_{n+1}-\boldsymbol{\Gamma}\cdot\frac{\partial\tilde{\boldsymbol{\varepsilon}}_{n+1}}{\partial\boldsymbol{\sigma}_{n+1}}:\Delta\boldsymbol{\sigma}\right)\Delta t.
\end{aligned}
\tag{34e}
$$

The shape of inclusion phase in Pierard et al. [15] is spherical. For comparison, the material parameters are kept as the same as those in Pierard et al. [15], and they are listed in Table 1. Figures 3 and 4 show the stress-strain responses of the composites under uniaxial tension with 15% and 30% volume fractions of inclusion phase, respectively. Curves obtained at four different strain rates, i.e., 1×10^{-6}, 1×10^{-5}, 1×10^{-4} and 1×10^{-3} s^{-1} are included in each figure. Figure 5(a) and (b) shows the cyclic stress-strain responses of the composite with 30% volume fraction of inclusion phase at the strain rates of 1×10^{-3} and 1×10^{-6}, respectively. It is seen that the predicted macroscopic stress-strain responses given by three classical linearization approaches (i.e., direct, secant and tangent ones) almost coincide with each other and are stiffer than that from the full-field finite element simulation. Although the tangent approach is much more complex, it does not give a better prediction. The reason can be explained from Figure 6, which shows the evolutions of the ratio $\Delta\mathbf{E}^{\mathrm{b}}_{11}/(\overline{\mathbf{M}}:\Delta\boldsymbol{\Sigma})_{11}$ (noted that the 1-1 direction is the loading direction) during the tensile deformation at a strain rate of 1×10^{-3} s^{-1}. It is seen that at the beginning of deformation, the ratio is equal to zero since only elastic deformation occurs, i.e., $\Delta\mathbf{E}^{\mathrm{b}}_{11}=\mathbf{0}$. However, the ratio increases with the increasing strain and beyond 1 when the strain reaches about 3.2%. In the subsequent deformation, the macroscopic strain increment $\Delta\mathbf{E}$ is dominated by $\Delta\mathbf{E}^{\mathrm{b}}$, rather than $\overline{\mathbf{M}}:\Delta\boldsymbol{\Sigma}$. In other words, the effective compliance tensors derived by the secant and tangent approaches, i.e., $\overline{\mathbf{M}}^{\mathrm{sec}}$ and $\overline{\mathbf{M}}^{\tan}$ are very close to the elastic compliance tensor $\overline{\mathbf{M}}^{\mathrm{e}}$ and the interaction between the matrix and inclusion phases is overestimated. From Figures 3(d), 4(d), 5(a) and (b), it is seen that the predicted results given by the new proposed mapping-tangent linearization approach is softer than those given by three classical approaches, and is much closer to that from the full-field finite element simulation. The ratio $\Delta\mathbf{E}^{\mathrm{b}}_{11}/(\overline{\mathbf{M}}:\Delta\boldsymbol{\Sigma})_{11}$ keeps as zero during the deformation since the mapping tensor $\boldsymbol{\Gamma}$ is determined by assuming that the back-extrapolated term in the affine relationship equals to zero. Under this condition, the overestimated interaction between the matrix and inclusion phases is reasonably reduced.

It should be noted that in Pierard et al. [15], the viscosity of the composite is very strong since the viscosity coefficient is set as a very small value (i.e., m=1.5). In this work, the predictive capabilities of different linearization approaches in the case of weak viscosity are also discussed. The materials parameters for the composite with a weak viscosity are listed in Table 2. However, owing to the lack of full-field results, some new finite element simulations are performed here. The inclusion repartition is assumed isotropic, as shown in Figure 7(a). Then, the composite can be characterized by the representative volume element (RVE), as shown in Figure 7(b). The finite element code ABAQUS is employed with the choice of 65472 hexahedron solid elements (C3D8). The finite element model of the RVE with elements is shown in Figure 7(c) (noted that in Figure 7(c) part of the matrix is removed to show the inclusion), where a spherical inclusion is assumed to be surrounded by a cubic matrix and the volume fraction of the inclusion is 30%. Meanwhile, the periodic boundary conditions are imposed on the cube surface of the finite element model in order to obtain more reasonable results:

$$
\begin{aligned}
&\mathbf{u}(x_1,x_2,0)-\mathbf{u}_3=\mathbf{u}(x_1,x_2,L),\\
&\mathbf{u}(x_1,0,x_3)-\mathbf{u}_2=\mathbf{u}(x_1,L,x_3),\\
&\mathbf{u}(0,x_1,x_2)-\mathbf{u}_1=\mathbf{u}(L,x_1,x_2),
\end{aligned}
\tag{35}
$$

where $\mathbf{u}$ is the displacement vector, L is the length of the RVE. In the finite element simulations, tensile loading is

Table 1 Material parameters used for the matrix and inclusion phases with a strong viscosity

	E (GPa)	v	σ_Y (MPa)	k (GPa)	d	γ_0 (s^{-1})	m
Matrix	70	0.330	70	4	0.40	3×10^{-4}	1.5
Inclusion	400	0.286	400	8	0.40	2×10^{-4}	1.5

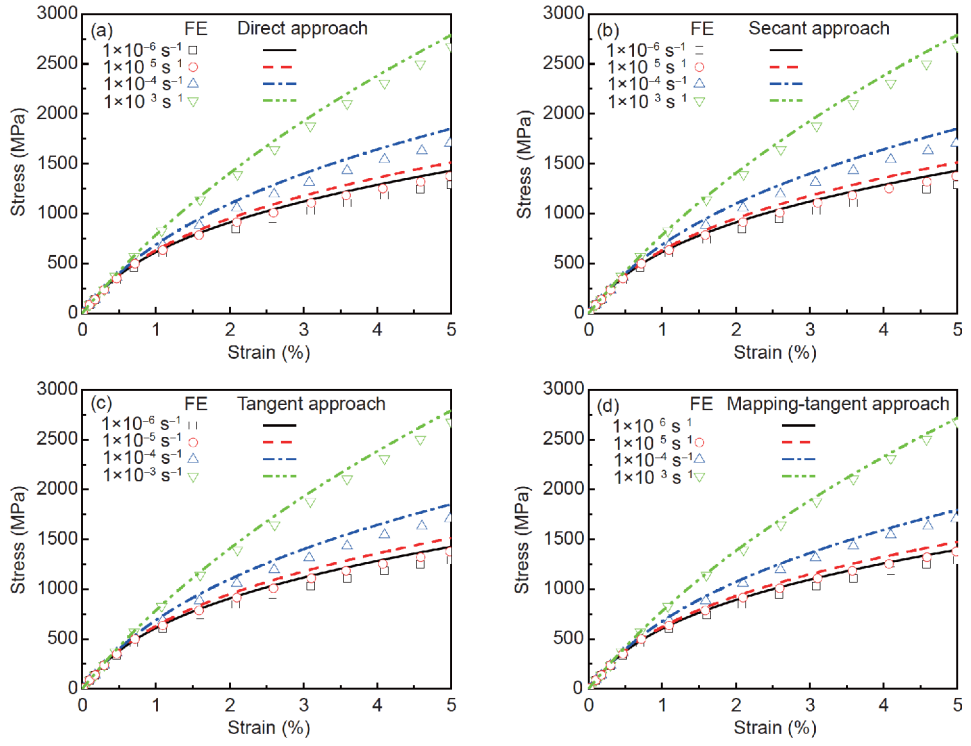

Figure 3 (Color online) Tensile stress-strain curves given by finite-element method [15] and self-consistent homogenization scheme based on different linearization approaches (the volume fraction of inclusion phase is 15%, the strain rates are 1×10^{-6}, 1×10^{-5}, 1×10^{-4} and 1×10^{-3} s^{-1}). (a) Direct approach; (b) secant approach; (c) tangent approach; (d) new proposed mapping-tangent approach.

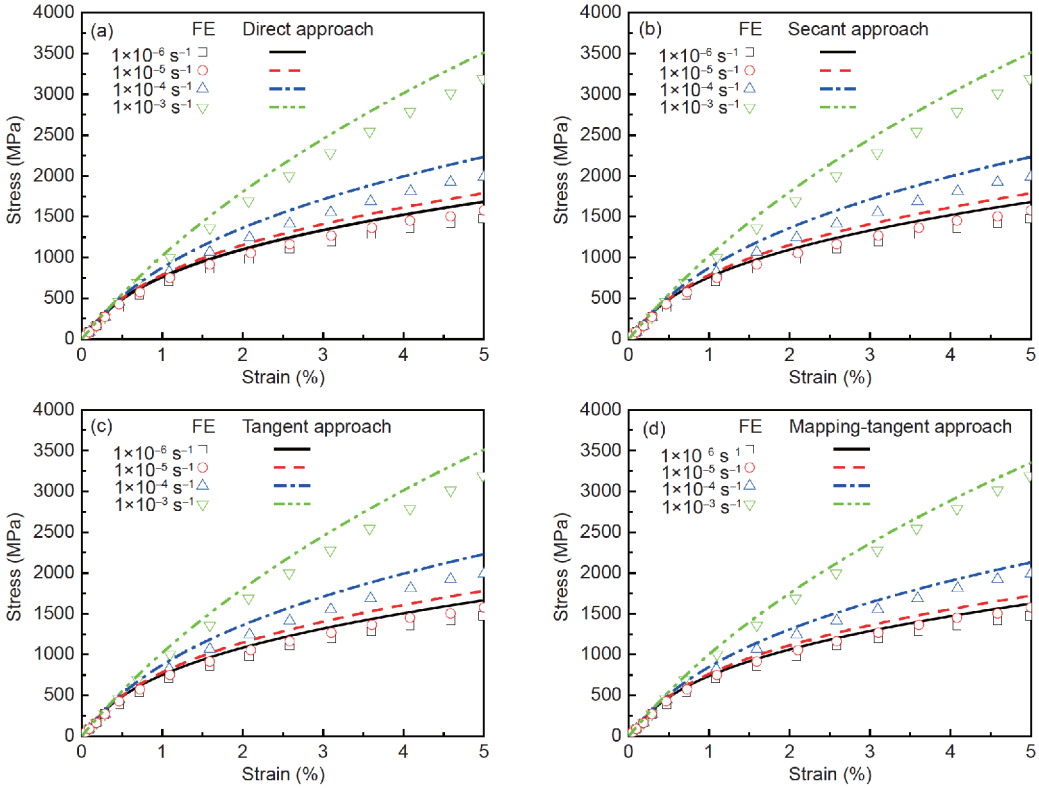

Figure 4 (Color online) Tensile stress-strain curves given by finite-element method [15] and self-consistent homogenization scheme based on different linearization approaches (the volume fraction of inclusion phase is 30%, the strain rates are 1×10^{-6}, 1×10^{-5}, 1×10^{-4} and 1×10^{-3} s^{-1}). (a) Direct approach; (b) secant approach; (c) tangent approach; (d) new proposed mapping-tangent approach.

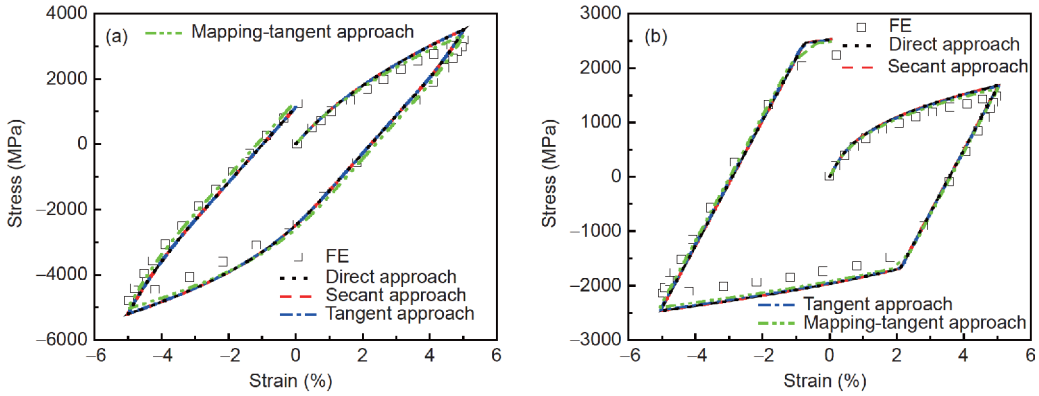

Figure 5 (Color online) Cyclic stress-strain responses given by finite-element method [15] and self-consistent homogenization scheme based on different linearization approaches (the volume fraction of inclusion phase is 30%). (a) At a strain rate of 1×10^{-3}; (b) at a strain rate of 1×10^{-6}.

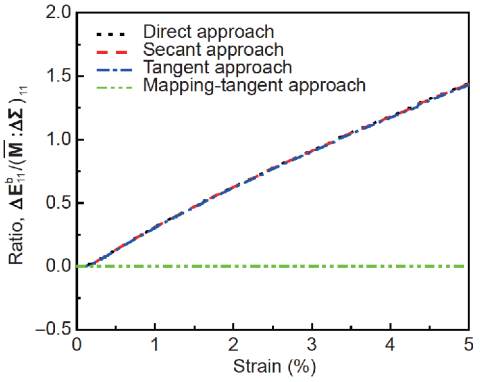

Figure 6 (Color online) Evolutions of the ratio $\Delta\mathbf{E}^{b}_{11}/(\overline{\mathbf{M}}:\Delta\boldsymbol{\Sigma})_{11}$ for the composite with 30% volume fraction of inclusion phase during the tensile deformation at a strain rate of 1×10^{-3}.

applied along the x_3 direction of the RVE. In this case, $\mathbf{u}_3=(0,0,\varepsilon L)$, $\mathbf{u}_1=(u_1,0,0)$ and $\mathbf{u}_2=(0,u_2,0)$, where ε is the applied engineering strain and u_1 and u_2 are computed from the condition that the total force acting on the cube surface has normal vectors perpendicular to x_3 is zero. The overall stress and strain are obtained by performing a volume average of the stress and strain fields in the RVE.

Figures 8(a) and 9(a) show the stress-strain responses of the composite under the uniaxial tension with 30% volume fraction of inclusion phase. The loading rates are 1×10^{-6} and 1×10^{-3} s^{-1}, respectively. It is seen that no noticeable difference between the results obtained by the direct and secant approaches. The direct and secant approaches provide very stiff predictions, but the mapping-tangent approach provides a soft one. The tangent approach gives the prediction between that by the direct/secant and mapping-tangent approaches. Comparing with the full-field finite element results, it can be concluded that the predicted results given by the new proposed linearization method is more reasonable than the three classical approaches. Figures 8(b) and 9(b) show the evolutions of the ratio $\Delta\mathbf{E}^{b}_{11}/(\overline{\mathbf{M}}:\Delta\boldsymbol{\Sigma})_{11}$ under two different loading rates.

5 Summary and conclusions

Using the fully implicit backward Euler's integration algo-

Table 2 Material parameters used for the matrix and inclusion phases with a weak viscosity

	E (GPa)	ν	σ_Y (MPa)	k (GPa)	d	γ_0 (s^{-1})	m
Matrix	70	0.330	70	1.5	0.40	3×10^{-4}	50
Inclusion	400	0.286	400	8	0.40	2×10^{-4}	50

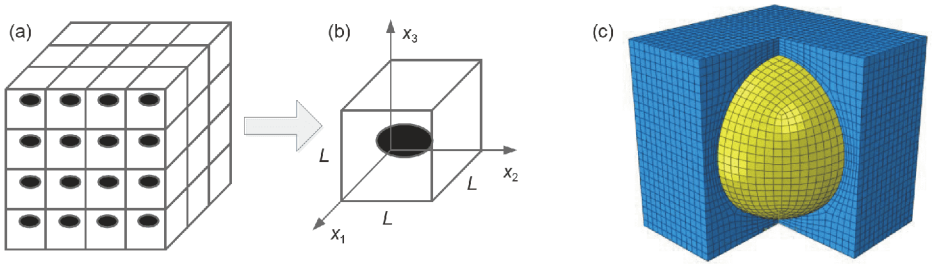

Figure 7 (Color online) (a) A square periodic array of inclusions to represent an isotropic spatial repartition; (b) representative volume element (RVE); (c) finite element mesh of the RVE.

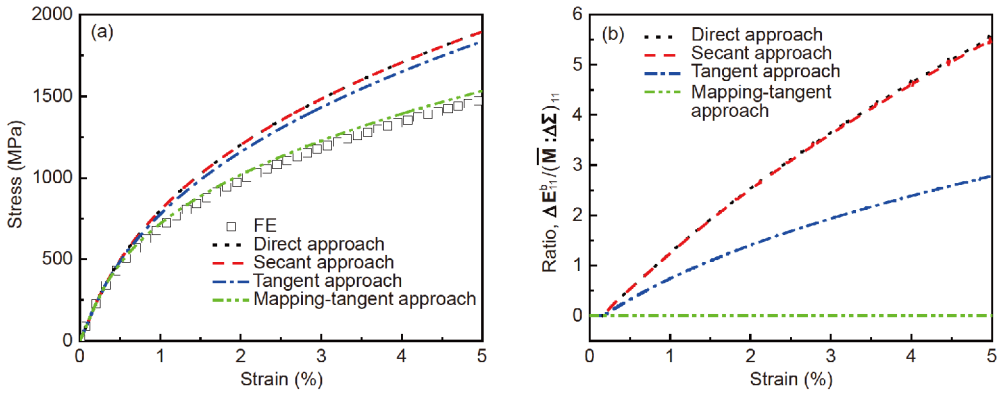

Figure 8 (Color online) Tensile stress-strain curves given by the finite element method and self-consistent homogenization scheme based on different linearization approaches for the composite with a weak viscosity (the volume fraction of inclusion phase is 30%, the strain rate is 1×10^{-6}). (a) Stress-strain curves; (b) evolutions of the ratio $\Delta\mathbf{E}^{b}_{11}/(\overline{\mathbf{M}}:\Delta\boldsymbol{\Sigma})_{11}$.

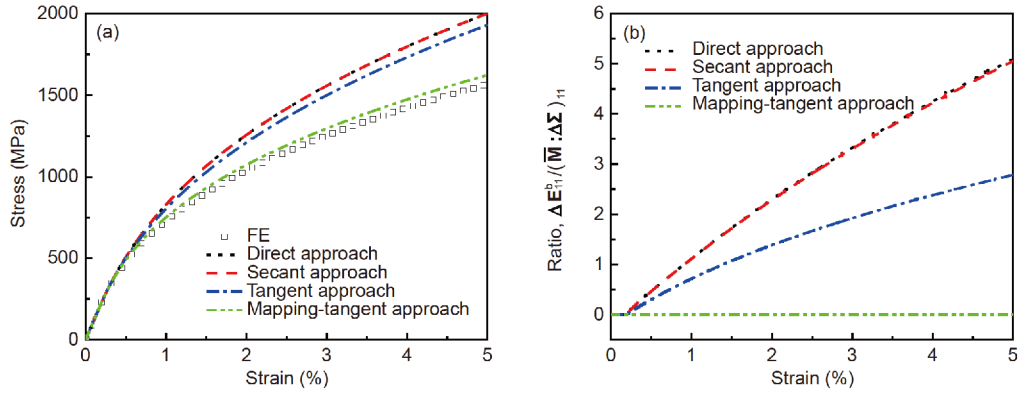

Figure 9 (Color online) Tensile stress-strain curves given by the finite element method and self-consistent homogenization scheme based on different linearization approaches for the composite with a weak viscosity (the volume fraction of inclusion phase is 30%, the strain rate is 1×10^{-3}). (a) Stress-strain curves; (b) evolutions of the ratio $\Delta\mathbf{E}^{b}_{11}/(\overline{\mathbf{M}}:\Delta\boldsymbol{\Sigma})_{11}$.

rithm, the nonlinear constitutive equations of the matrix and inclusion phases in the composites are discretized. Three classical incremental linearization approaches, i.e., direct, secant and tangent ones are adopted and affine relationships between the stress and strain increments are deduced. A new mapping-tangent linearization approach is proposed in order to weaken the interaction between the matrix and inclusion phases. Different linearization approaches are implemented by the incremental self-consistent scheme to predict the overall responses of particle-reinforced composites. The main conclusions are listed as follows.

(1) Numerical results show that when the viscosity of the composites is strong, the predicted stress-strain curves given by three classical linearization approaches are much stiffer than that from the full-field finite element simulation; but the new proposed mapping-tangent linearization approach provides a softer prediction, which is much closer to that from the full-field simulations.

(2) When the viscosity of the composites is weak, the direct and secant approaches provide very stiff predictions, but the mapping-tangent approach gives a soft prediction, and the tangent approach provides a prediction between that by the direct/secant and mapping-tangent approaches.

(3) In the classical linearization approaches (i.e., direct, secant and tangent ones), the macroscopic strain increment $\Delta\mathbf{E}$ is dominated by $\Delta\mathbf{E}^{b}$ rather than $\overline{\mathbf{M}}:\Delta\boldsymbol{\Sigma}$ when the deformation is large, which results in a strong interaction between the matrix and inclusion phases. Thus, the basic idea of this work is to eliminate the back-extrapolated term in the affine relationship of stress and strain increments by introducing a new mapping tensor.

(4) The linearized constitutive equation based on the proposed mapping-tangent approach has the same mathematical structure as the rate-independent elasto-plastic constitutive law. So, the homogenization problems faced in the elasto-plastic and elasto-viscoplastic heterogeneous materials can be unified.

In the future work, the proposed mapping-tangent linearization approach will be extended to describe the cyclic deformation of the composites and polycrystalline aggregates by introducing the back stress into the constitutive equations.

This work was supported by the National Natural Science Foundation of China (Grant Nos. 11602203, 11532010), the Young Elite Scientist Sponsorship Program by CAST (Grant No. 2016QNRC001), and the Fundamental Research Funds for the Central Universities (Grant No. 2682018CX43).

1 Eshelby J D. The determination of the elastic field of an ellipsoidal inclusion, and related problems. Proc R Soc A-Math Phys Eng Sci, 1957, 241: 376–396
2 Kröner E. Berechnung der elastischen konstanten des vielkristalls aus den konstanten des einkristalls. Z Physik, 1958, 151: 504–518
3 Mori T, Tanaka K. Average stress in matrix and average elastic energy of materials with misfitting inclusions. Acta Metall, 1973, 21: 571–574
4 Hill R. A self-consistent mechanics of composite materials. J Mech Phys Solids, 1965, 13: 213–222
5 Hill R. Continuum micro-mechanics of elastoplastic polycrystals. J Mech Phys Solids, 1965, 13: 89–101
6 Hutchinson J W. Bounds and self-consistent estimates for creep of polycrystalline materials. Proc R Soc A-Math Phys Eng Sci, 1976, 348: 101–127
7 Hutchinson J W. Elastic-plastic behaviour of polycrystalline metals and composites. Proc R Soc A-Math Phys Eng Sci, 1970, 319: 247–272
8 Molinari A, Canova G R, Ahzi S. A self consistent approach of the large deformation polycrystal viscoplasticity. Acta Metall, 1987, 35: 2983–2994
9 Doghri I, Ouaar A. Homogenization of two-phase elasto-plastic composite materials and structures. Int J Solids Struct, 2003, 40: 1681–1712
10 Nemat-Nasser S, Obata M. Rate-dependent, finite elasto-plastic deformation of polycrystals. Proc R Soc A-Math Phys Eng Sci, 1986, 407: 343–375
11 Peng X, Hu N, Zheng H, et al. Evaluation of mechanical properties of particulate composites with a combined self-consistent and Mori-Tanaka approach. Mech Mater, 2009, 41: 1288–1297
12 Peng X, Hu N, Long X, et al. Extension of combined self-consistent and Mori-Tanaka approach to evaluation of elastoplastic property of particulate composites. Acta Mech Solid Sin, 2013, 26: 71–82
13 Masson R, Zaoui A. Self-consistent estimates for the rate-dependent elastoplastic behaviour of polycrystalline materials. J Mech Phys Solids, 1999, 47: 1543–1568
14 Pierard O, Doghri I. An enhanced affine formulation and the corresponding numerical algorithms for the mean-field homogenization of elasto-viscoplastic composites. Int J Plast, 2006, 22: 131–157
15 Pierard O, LLorca J, Segurado J, et al. Micromechanics of particle-reinforced elasto-viscoplastic composites: Finite element simulations versus affine homogenization. Int J Plast, 2007, 23: 1041–1060
16 Molinari A, Ahzi S, Kouddane R. On the self-consistent modeling of elastic-plastic behavior of polycrystals. Mech Mater, 1997, 26: 43–62
17 Mercier S, Molinari A. Homogenization of elastic-viscoplastic heterogeneous materials: Self-consistent and Mori-Tanaka schemes. Int J Plast, 2009, 25: 1024–1048
18 Wang H, Wu P D, Tomé C N, et al. A finite strain elastic-viscoplastic self-consistent model for polycrystalline materials. J Mech Phys Solids, 2010, 58: 594–612
19 Mercier S, Molinari A, Berbenni S, et al. Comparison of different homogenization approaches for elastic-viscoplastic materials. Model Simul Mater Sci Eng, 2012, 20: 024004
20 Wang H, Capolungo L, Clausen B, et al. A crystal plasticity model based on transition state theory. Int J Plast, 2017, 93: 251–268
21 Turner P A, Tomé C N. Self-consistent modeling of visco-elastic polycrystals: Application to irradiation creep and growth. J Mech Phys Solids, 1993, 41: 1191–1211
22 Turner P A, Tomé C N, Woo C H. Self-consistent modelling of nonlinear visco-elastic polycrystals: An approximate scheme. Philos Mag A, 1994, 70: 689–711
23 Doghri I, Adam L, Bilger N. Mean-field homogenization of elasto-viscoplastic composites based on a general incrementally affine linearization method. Int J Plast, 2010, 26: 219–238
24 Miled B, Doghri I, Brassart L, et al. Micromechanical modeling of coupled viscoelastic-viscoplastic composites based on an incrementally affine formulation. Int J Solids Struct, 2013, 50: 1755–1769
25 Wu L, Adam L, Doghri I, et al. An incremental-secant mean-field homogenization method with second statistical moments for elasto-visco-plastic composite materials. Mech Mater, 2017, 114: 180–200
26 Chaboche J, Kanoute P, Roos A. On the capabilities of mean-field approaches for the description of plasticity in metal matrix composites. Int J Plast, 2005, 21: 1409–1434
27 Peng X, Tang S, Hu N, et al. Determination of the Eshelby tensor in mean-field schemes for evaluation of mechanical properties of elastoplastic composites. Int J Plast, 2016, 76: 147–165